



Identifying the photoproduction sites of reactive oxygen species in dissolved black carbon: A remarkable role of oxygenated functional groups

Lin Wang ^{a,b}, Hao Jiang ^a, Jun Zhang ^{a,c}, Xinhua He ^d, Fangfang Li ^{a,*}, Jing Feng ^{b,**}, Bo Pan ^a

^a Yunnan Provincial Key Laboratory of Soil Carbon Sequestration and Pollution Control, Faculty of Environmental Science & Engineering, Kunming University of Science & Technology, Kunming 650500, China

^b Faculty of Material Science and Engineering, Kunming University of Science and Technology, Kunming 650500, China

^c Agronomy College, Shenyang Agricultural University, Shenyang 110866, China

^d School of Biological Sciences, University of Western Australia, Perth, WA 6009, Australia



ARTICLE INFO

Keywords:

Dissolved black carbon
Reactive oxygen species
Carbonyls
Ethers
Non-electron transfer

ABSTRACT

Dissolved black carbon (DBC) can generate reactive oxygen species (ROS), playing significant roles in contaminants degradation and chemical stresses to microorganisms. However, little is known regarding the photoproduction sites to ROS generation, mainly because of its extremely complicated composition. Herein, the ROS generation and photoexcited alteration of DBC were investigated. The generation mechanisms of hydroxyl radical ($\bullet\text{OH}$), superoxide anion (O_2^\bullet), and singlet oxygen (${}^1\text{O}_2$) were inferred by employing various model chemicals. Results showed that the photo-excited aliphatic carbonyls greatly contributed to $\bullet\text{OH}$, O_2^\bullet , and ${}^1\text{O}_2$ generation. Ether groups were identified as the main structural source of H_2O_2 -dependent $\bullet\text{OH}$ generation. The novel non-electron transfer process involved carbonyl, ether, alcohol, and ester groups to produce O_2^\bullet was proposed. These findings reveal the vital role of oxygenated functional groups within DBC in the photoactive generation of ROS, and thus provides new theoretical information for DBC's environmental geochemical behavior.

1. Introduction

Black carbon (BC) is produced by incomplete combustion of biomass, fossil fuels and vegetation [1]. Escalating anthropogenic activities in coastal and estuarine environments are resulting in increased exposure to BC in nearshore environments [2]. BC persists on timescales of centuries to millennia, and is very effective at absorbing light in the environment. The soluble components in BC (dissolved black carbon, DBC) can be readily mobilized from soils by infiltration and surface runoff. DBC accounts for 10 % of the global riverine flux of dissolved organic carbon, being an terrestrial BC input to dissolved organic matter (DOM) in water bodies [3]. As an important constituent of DOM pool, DBC can absorb photons and photoexcite to excited state, then subsequently interact with water molecules or transfer energy to dissolved oxygen to produce reactive oxygen species (ROS) [4–6]. ROS from DBC can promote the phototransformation of organic contaminants [7,8], regulate the geochemical behavior of heavy metals [9,10], damage the cell

membrane or cellular walls [11,12], and exacerbate the photodamage of extracellular DNA [12]. The photochemistry of DBC is thus vital to understand its own fate and that of priority pollutants.

Exploring the generation mechanisms of ROS by DBC has enormous influence on the environmental transformation of pollutants and the exploring of biogenetic pathology. To investigate the mechanisms of ROS generation, it is essential to identify the determining structures of DBC for ROS generation. However, to date, there is rare information about the photoproduction sites of ROS in DBC. Some works on structural identification of DOM to ROS generation mechanisms indicated the contribution of quinone to $\bullet\text{OH}$ generation, the positive correlation between ${}^1\text{O}_2$ production and E2/E3 ratio (A254 divided by A365), and the formation of O_2^\bullet by obtaining electron from phenolic groups. However, due to the few concentrations of quinones in DOM, the contribution of quinone structure to $\bullet\text{OH}$ generation was queried by later studies [13–15]. Moreover, although it has known that the formation of ${}^1\text{O}_2$ partly due to ${}^3\text{DOM}^*$ energy transfer to O_2 [16], the

* Correspondence to: Yunnan Provincial Key Laboratory of Soil Carbon Sequestration and Pollution Control, Faculty of Environmental Science & Engineering, Kunming University of Science & Technology, No. 727 Jingming South Rd, Kunming, 650500, China.

** Correspondence to: Faculty of Material Science and Engineering, Kunming University of Science and Technology, Kunming 650093, China.

E-mail addresses: fangkust@163.com (F. Li), jingfeng@kmust.edu.cn (J. Feng).

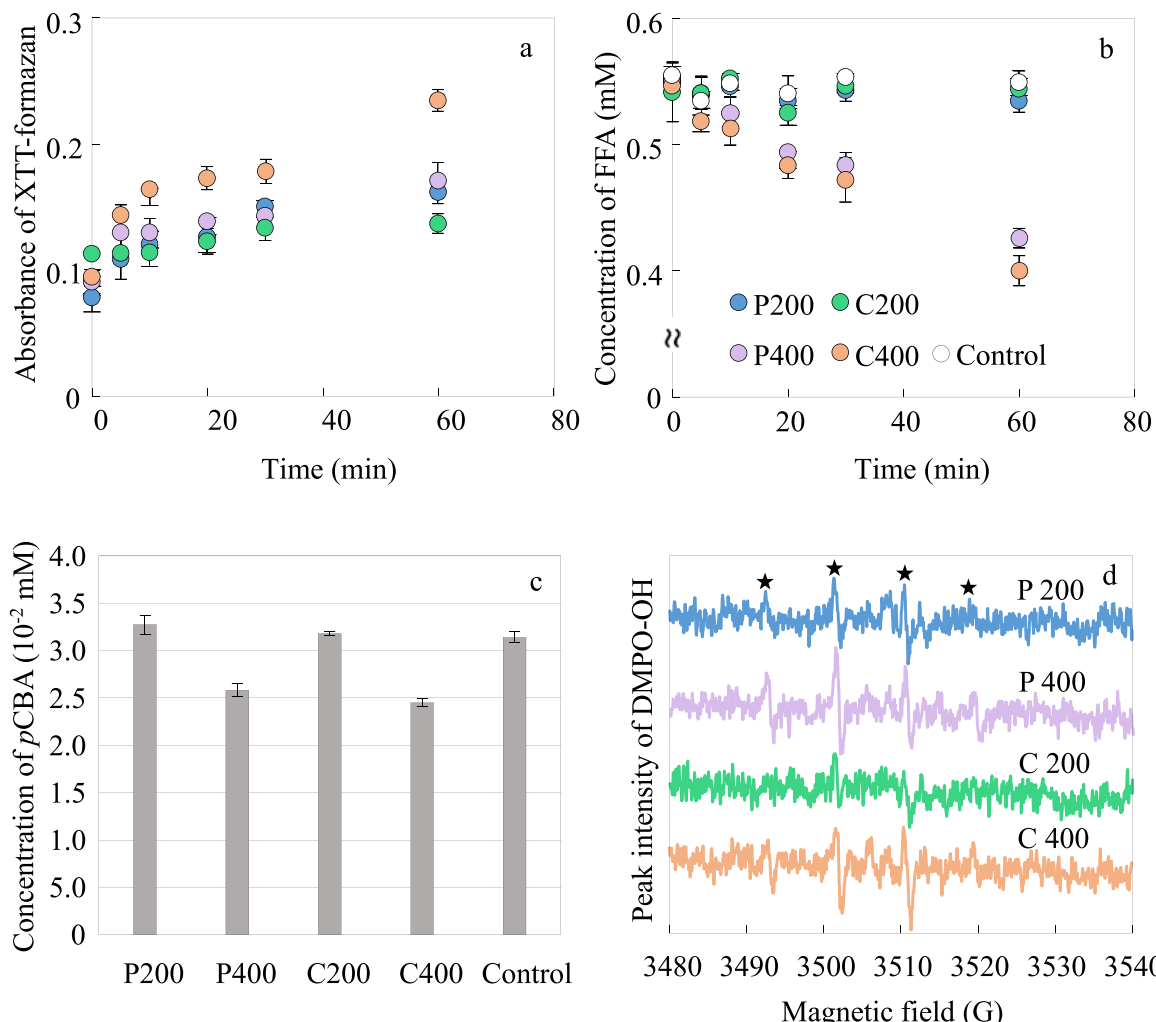


Fig. 1. Production of O_2^- , $^1\text{O}_2$, or $\bullet\text{OH}$ by DBCs under UV irradiation as indicated by the reduction of XTT (a), FFA (b), *p*CBA (c), and the EPR signal of DMPO-OH (d), respectively.

identification about the structures within DOM to $^3\text{DOM}^*$ formation is still lacking. Furthermore, due to the ban of quantum rules, the interpretation about O_2^- generation through direct electron transfer from phenolic groups to ground state O_2 ($^3\text{O}_2$) is still obscure. As a natural compound, DBC consists of various functional groups and components. Because of the extremely complex structures, it is difficult to identify the photoproduction sites of ROS in DBC. How the organic moieties (structures) within DBC related to ROS generation is still unknown, and this line of research is also generally lacking.

To identify the photoproduction sites and photoactive generation mechanisms of DBC in the generation of ROS ($\bullet\text{OH}$, $^1\text{O}_2$ and O_2^-), the objectives of this study were to address or quantify (i) the production of $\bullet\text{OH}$, $^1\text{O}_2$ and O_2^- from DBC; (ii) the structural alterations of DBC; (iii) the specific roles of functional groups within DBC to the generation of individual ROS; and (iv) the generation mechanism of ROS from DBC by employing various model chemicals. Based on the structural alteration of DBC after UV irradiation and model chemicals with different functional groups, ROS generation mechanisms could be correlated to the specific structural characteristics of DBC.

2. Materials and methods

2.1. Chemicals

All of the chemicals (higher than analytical grade) of 5,5-Dimethyl-1-

pyrrolidine N-oxide (DMPO, 98 %), furfuryl alcohol (FFA, 98 %), 2,3-bis (2-methoxy-4-nitro-5-sulfonylphenyl)-2H-tetrazolium-5-carboxanilide (XTT, ≥ 90 %), para-chlorobenzoic acid (*p*CBA, 99 %), diphenyl ether (99 %), 1,4-Benzoquinone and hydroquinone (99 %) were purchased from Sigma-Aldrich (U.S.A.). Ethylene glycol dimethyl ether (99 %), ethyl formate (99 %), phenyl acetate (99 %), glycerol (≥ 90 %), L-(-) glyceraldehyde (99 %), D-(-)fructose (99 %), propionic acid (99 %) and benzoic acid (99 %) were purchased from the Aladdin Reagent Company (Shanghai, China). Superoxide dismutase (SOD) was purchased from the Shanghai Yuanye Biotechnology Company (Yuanye, Shanghai, China).

2.2. Preparation of biochars and DBCs

Both corn straw and peanut shell for making biochar were collected in a local agricultural field from Kunming, Yunnan Province, China. Raw biomass was air dried before ground into powder by a high-speed pulverizer (BG-1001, Zhongshan Changbai Instrument, China). According to our preliminary experiments, biomasses were pyrolyzed at 200, 300, 400, and 500 °C, DBCs which were extracted from 200 °C and 400 °C biochars showed the higher carbon content and photochemical activity than DBCs from other temperatures. Thus, DBCs from 200 °C and 400 °C biochars were used in the phototransformation and ROS photoproduction site experiment. Biomasses were pyrolyzed at 200 °C or 400 °C in a muffle furnace under oxygen-limited conditions, the pyrolysis temperature was programmed to increase from 20 °C to 200/400 °C in 2 hours

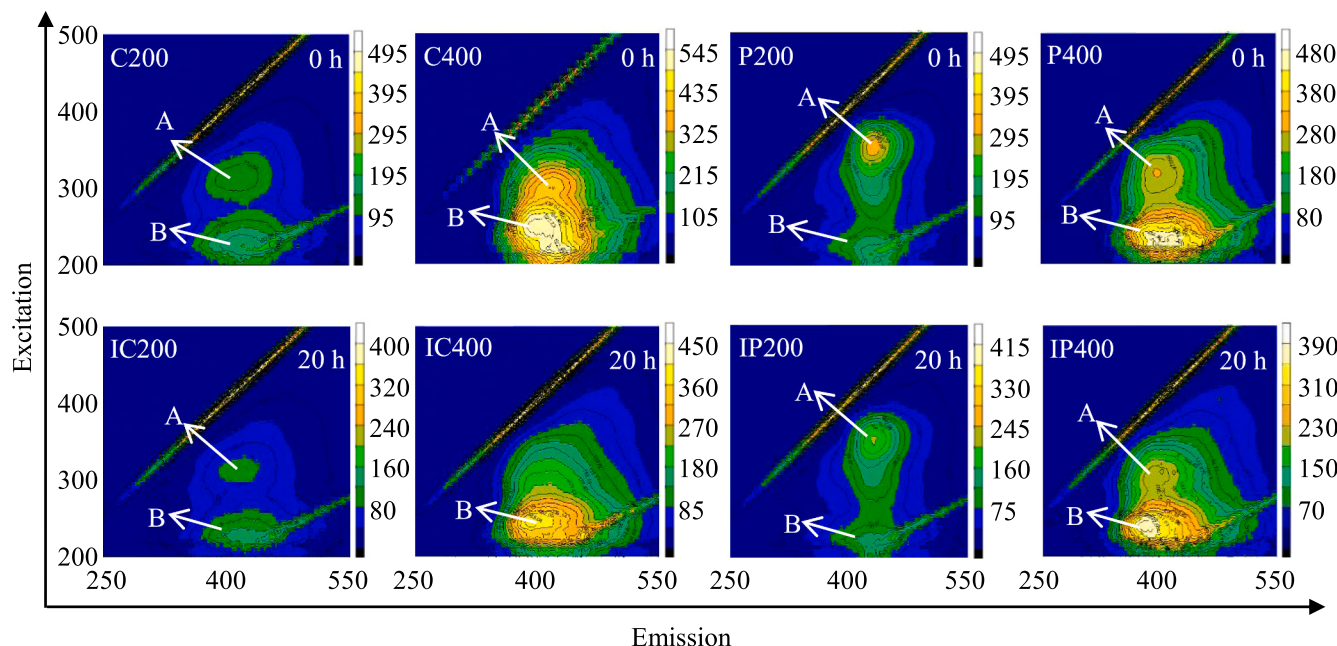


Fig. 2. Fluorescence excitation emission matrix (EEM) of 10 mg OC/L DBCs before and after 20 h UV light irradiation at 365 nm. IP and IC represent UV-irradiated DBCs from peanut shell biochars and from corn straw biochars, respectively.

and maintain at 200 °C or 400 °C for another 4 hours. The mixture of 100 g 100-mesh sieve (aperture 0.15 mm) biochar powder and 1000 mL deionized water was sonicated in a bath sonicator (KH-800TDB, Kunshan Hechuang Ultrasonic Instrument, Jiangsu, China) at 100 W for 30 min to abstract DBC. Filtrates that filtered through 0.45-μm nylon membrane (CNW ANPEL Inc., China) were operationally defined as DBCs. The residue retained on the membrane was collected and subjected to another two rounds of sonication and filtration. According to the biomass source (P as peanut shells, C as corn straws) and pyrolysis temperatures (200 °C or 400 °C), the extracted DBCs were named as P200, P400, C200, and C400, respectively. Every DBC solution was separate to two parts, one part was freeze-dried and grinded to analyze chemical characterizations, and the other was added to the photoreaction system after quantified by a TOC analyzer (Vario TOC APFA-370, Elementar).

The C, O, H, N, and S composition in the four freeze-dried DBCs were determined by an elemental analyzer (MicroCube, Elementar, Germany). The optical activity of chromophoric structures within DBCs before and after 20 h UV irradiation was investigated by UV-vis absorption (UV-2600, Shimadzu, Japan) and fluorescence response. Considering the detection limit of fluorescence spectrophotometer (LS55, PerkinElmer Inc.), 10 mg OC/L DBCs were used to measure the excitation-emission matrix (EEM), across the excitation (Ex) wavelengths of 200–500 nm and emission (Em) wavelengths of 250–550 nm. The slits for both excitation and emission were 5 nm with scan speed of 600 nm/min and time interval of 0.1 min at 750 V voltage. The characterization of DBCs before and after 20 h UV irradiation was further analyzed by ¹H nuclear magnetic resonance spectroscopy (NMR, Bruker BioSpin, Switzerland) at 600 MHz, and a fourier transform infrared (FTIR) spectrometer (Varian 640-IR) in the transmission mode using KBr pellet (0.2 mg HA in 200 mg KBr), the spectra were collected in the range of 4000–400 cm⁻¹ with 16 scans at a resolution of 8 cm⁻¹.

2.3. Determination of •OH, ¹O₂, and O₂^{•-}

The production of hydroxyl radical (•OH), superoxide anion (O₂^{•-}) and singlet oxygen (¹O₂) by four DBCs (25 mg OC/L) and model chemicals (40 mg C/L) during the 60 min UV light irradiation was quantified by the molecular probe method. Based on the sensitivity and

selectivity of trapping agents, the *p*-chlorobenzoic acid (pCBA, 35 μM), 100 μM XTT (2,3-bis(2-methoxy-4-nitro-5-sulfophenyl)-2 H-tetrazolium-5-carboxanilide), and 50 μM FFA (furfuryl alcohol) were used as the indicator for •OH, O₂^{•-}, and ¹O₂ respectively [17–19]. The reduction kinetics of pCBA, FFA and XTT under UV irradiation in the presence of DBCs were conducted at 20 °C. Phosphate buffer solution (PBS, pH = 8.5, 10 mM) was added into the photochemical reaction systems to weaken interference of the pH changing. Tubes were placed in a photochemical reactor (XPA-7, Nanjing Xujiang Electromechanical Plant, China) and rotated at 400 rpm, the 300-W high pressure mercury lamp with light filter was placed in a quartz cooling pipe positioned vertically in the center of the photochemical reactor. The wavelength of light source ranged from 350 to 450 nm and centered at 365 nm. The light intensity at 365 nm in the quartz colorimetric tube was 54.3 mWcm⁻². Prepared XTT stock solution (5 mM) in brown vial was stored in refrigerator at 4 °C, and available for next day. Time-dependent orange-colored XTT-formazan absorbances, which resulted from reduction of XTT by O₂^{•-} [18], were measured by a UV-Vis spectrophotometer (Shimadzu, DU2600) at 470 nm. The concentrations of pCBA and FFA were analyzed with a high-performance liquid chromatograph (HPLC, Agilent 1200, USA) equipped with a reversed-phase C8 column (5 mm, 4.6×150 mm) and a UV detector (236 nm for pCBA and 230 nm for FFA). The mobile phase for pCBA and FFA was 30: 70 (v: v) of acetonitrile and deionized water with 0.54% phosphoric acid, and the flow rate of the mobile phase was 1 mL min⁻¹. Retention time for pCBA and FFA were 4.5 min and 5 min, respectively.

Free radical signals of •OH from DBCs were trapped monitored using DMPO as spin-trapping agents. The reaction condition for the mixture of DBC and DMPO was confirmed according to the preliminary experiment results (Fig. S1). Prior to the trapping of spin adduct of •OH (DMPO-OH), the mixtures of 100 μL DBC solutions (50 mg OC/L) and 100 μL DMPO agent (43.33 g/L) were stored in a 1 mL vial with gap and reacted in dark for 24 h. The final concentrations of DBC in this reaction system were 25 mg OC/L. The intensities of spin trap signals of DMPO-OH were monitored by electron paramagnetic resonance (EPR) spectrometer (Bruker, A300-6/1, Germany) with a single cavity, a modulation of 100 kHz and microwave frequencies of 9.2–9.9 GHz. EPR microwave power was specifically set to 31 dB (or 0.131 mW) and the sweep time was 81.92 ms, and other equipment parameters for detecting were

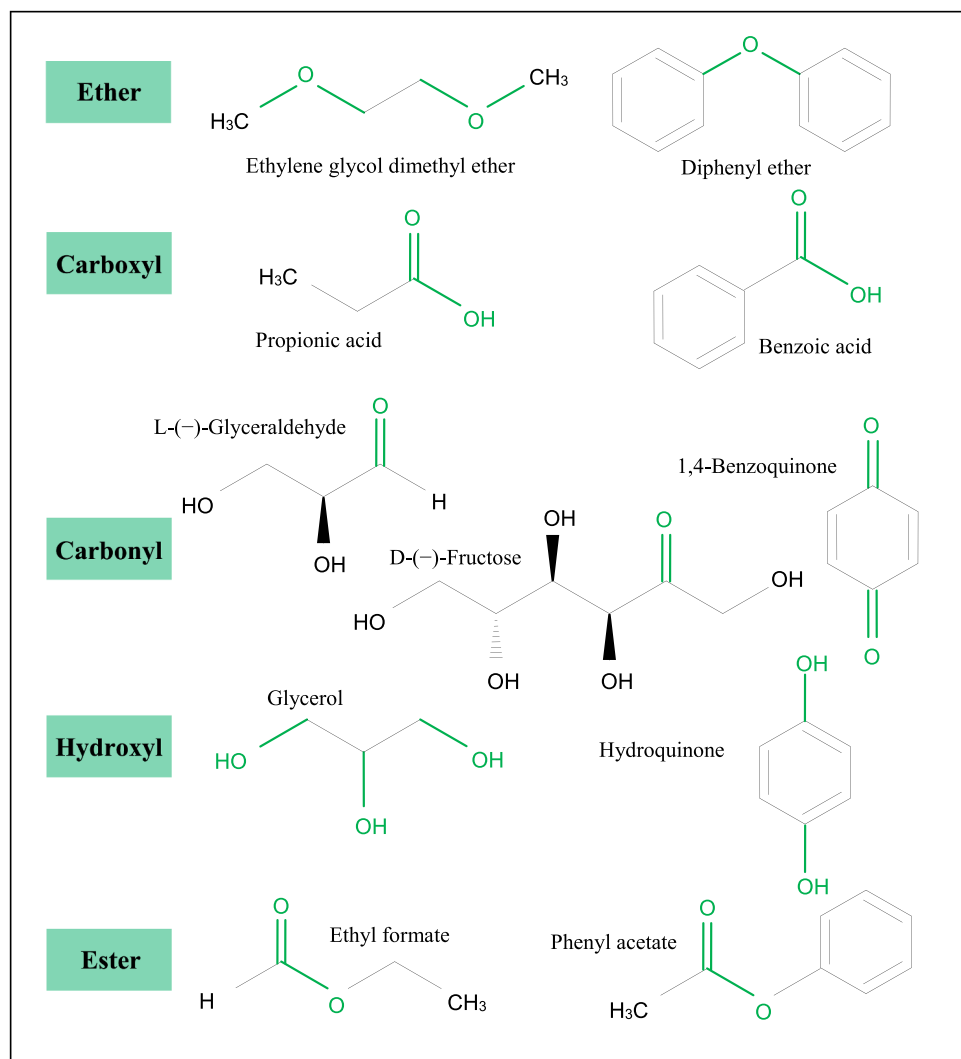


Fig. 3. Various model chemicals selected to identify the structural contribution in DBCs to ROS production.

setting as following: the sweep width was 100 G, the modulation amplitude was 1.00 G, and the resolution in the X axes was 1024 points.

3. Results and discussion

3.1. The generation of ROS in DBC systems

The generation kinetics of ROS (O_2^- , $\bullet\text{OH}$, and ${}^1\text{O}_2$) from DBCs are shown in Fig. 1. All the DBCs, especially C400, stimulated O_2^- production under UV irradiation, as reflected by the increasing absorbance of XTT-formazan (Fig. 1a, Table S1). However, the generations of ${}^1\text{O}_2$ and $\bullet\text{OH}$ were only observed in the two 400 °C DBCs, and the concentrations were higher in C400 than in P400, suggested by the obvious reduction of FFA and *p*CBA (Fig. 1b and 1c).

According to the elemental composition analysis of DBCs, the higher atomic ratios of (O/C) indicated that 400 °C DBCs contained more oxygenated functional groups (OFGs) (Table S2). Meanwhile, the fluorescence excitation emission matrix (EEM) of DBCs is presented in Fig. 2. The peak A in the region of excitation/emission (Ex/Em) = 315–355/400–435 nm is associated with humic acid-like molecules, and the peak B (Ex/Em = 220–230/400–425) is ascribed to fulvic acid-like molecules [20]. Two 400 °C DBCs showed the stronger response to fulvic acid-like groups than 200 °C DBCs (Table S3). Fulvic acid groups are consisted of multiple active OFGs, including carboxyl, phenolic-OH, alcoholic-OH and quinone groups [21,22]. Therefore, more significant ROS

production of P400/C400 could be attributed to their abundant photoactive OFGs, indicating a vital role of OFGs within DBCs in ROS generation. To further identify the structures responsible for ROS generation from DBC, more attention should be focused on the role of OFGs. To reduce the complexity of component in DBC, various model chemicals with OFGs in aliphatic carbon chains or aromatic rings were selected to examine ROS generation mechanisms. The model chemicals included diphenyl ether, ethylene glycol dimethyl ether, propionic acid, benzoic acid, L-(-)-glyceraldehyde, D-(-)-fructose, 1,4-benzoquinone, glycerol, hydroquinone, and ethyl formate, phenyl acetate (Fig. 3). These organic molecules have simple oxygen-containing structures, and good solubilities in water. Thus, they were selected to model the intrinsic structures of ether, carboxyl, carbonyl, hydroxyl, and ester within DBCs at a molecular level.

3.2. Structural identification of DBCs associated with ROS generation

Based on the time-dependent degradation of *p*CBA in the presence of model chemicals, we speculated that the structures of quinones, phenolic groups, aliphatic carbonyls, ethers may be related to $\bullet\text{OH}$ generation (the reduction efficiency of *p*CBA > 98 %, Fig. 4a, Table S4). Earlier work considered quinonoid and phenolic moieties within DOM as the main components in producing $\bullet\text{OH}$ [15,23], which was observed in this work using hydroquinone and 1,4-benzoquinone. However, the liquid-state ${}^1\text{H}$ NMR and FTIR spectra for DBCs showed little quinones

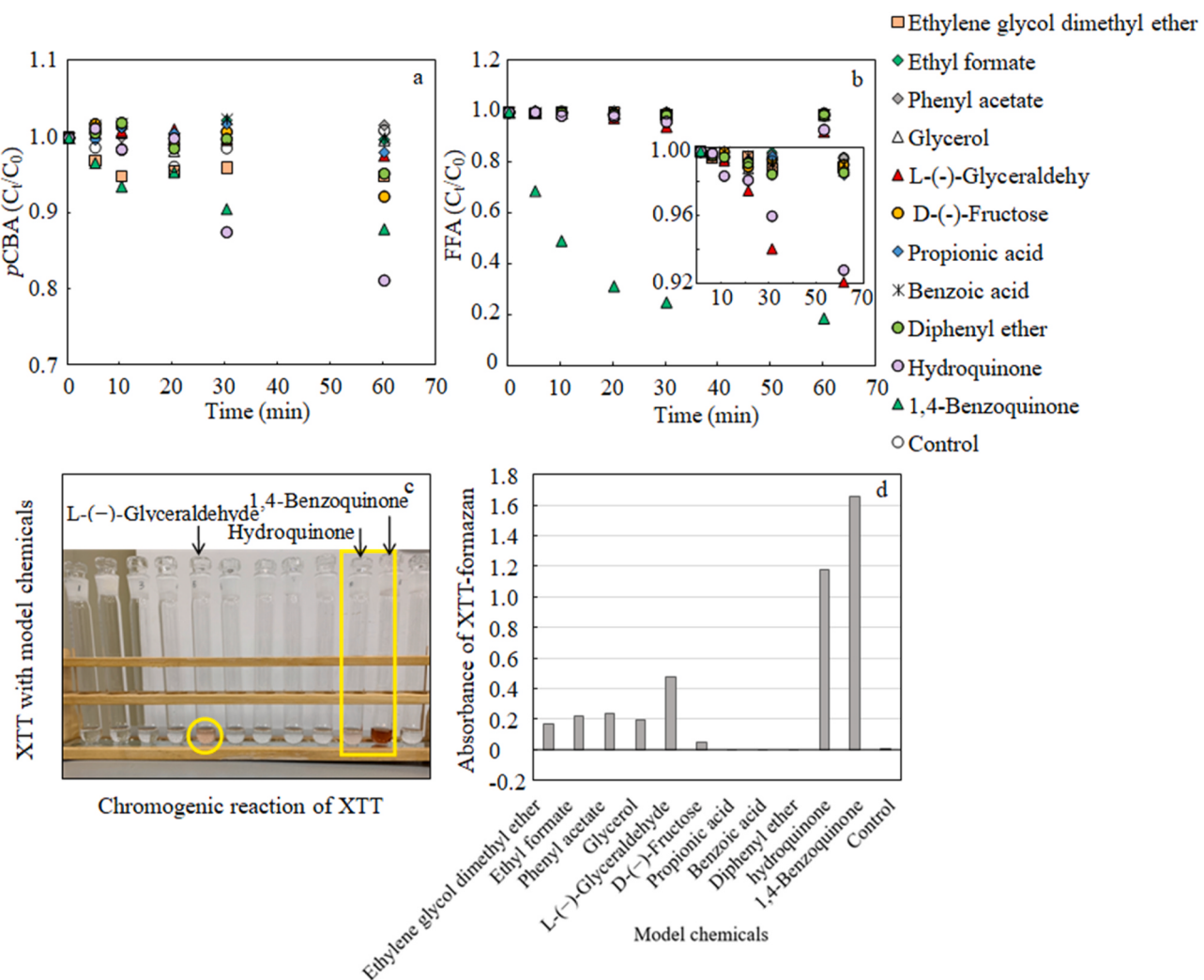


Fig. 4. The $\bullet\text{OH}$ generation kinetics indicated by the degradation of 30 μM pCBA by model chemicals under UV irradiation (a). The $^1\text{O}_2$ generation kinetics indicated by the degradation of 50 μM FFA by model chemicals under UV irradiation (b). The chromogenic reaction of XTT (0.1 mM) in the presence of model chemicals after 60 min UV irradiation (c). The generation of O_2^- indicated by the reduction of 100 μM XTT in the presence of model chemicals (d).

Table 1

Composition of functional groups (in % of total H) in before and after UV irradiation DBCs obtained by liquid-state ^1H NMR spectra.^a

Sample	0.5–2.8 Aliphatic	2.3–2.4 Ketone	3–4.5 Carbohydrate	3.11 Ether	3.92 Peroxide	1.9, 8.44 Ester	5.0–6.0 Olefins/ 2.9–3.0 Alkyne	6.0–8.0 Aromatic	6.8 Quinone	5.35 Phenolic -OH
P200	9.41	1.48	52.15	N.D.	1.61	10.75	4.03	20.56	N.D.	N.D.
P400	14.93	14.93	34.33	N.D.	2.99	26.87	N.D.	5.97	N.D.	N.D.
C200	37.31	0.68	45.74	0.36	3.31	11.29	0.23	1.09	N.D.	N.D.
C400	16.09	9.20	1.15	2.30	5.75	11.49	5.75	48.28	N.D.	N.D.
IP200	28.46	2.38	51.16	N.D.	4.38	13.63	N.D.	N.D.	N.D.	N.D.
IP400	39.53	N.D.	2.33	N.D.	N.D.	58.14	N.D.	N.D.	N.D.	N.D.
IC200	50.27	0.31	44.51	0.27	4.20	0.45	N.D.	N.D.	N.D.	N.D.
IC400	38.46	N.D.	3.85	N.D.	N.D.	57.69	N.D.	N.D.	N.D.	N.D.

^a N.D. represents non-detectable. IP and IC represent DBCs from peanut shell biochars and from corn straw biochars after a 20 h UV irradiation, respectively.

and phenols (Fig S3-S6, Table 1 and Fig. 5). In addition, due to the low concentration of quinones in DOM, the contribution of quinones to $\bullet\text{OH}$ generation was also queried by a series of later studies [13–15]. Thus, the quinone and phenolic groups within DBC played a relatively minimal role in ROS generation.

The aliphatic carbonyls and ethers groups were substantially detected by ^1H NMR and FTIR spectra. Considering the significant content of these two structures in DOM [24,25], their stimulated $\bullet\text{OH}$ generation

deserved more attention than quinones. In the ^1H NMR spectra of DBCs (Fig S3-S6), the typical sharp peaks from 2.3 to 2.4 ppm could be assigned to α -methyl protons in ketones [26,27] with the range of 0.68–14.93 % (Table 1). The content of ether groups within DBCs was analyzed by both ^1H NMR quantification (Table 1) and FTIR signals at 1087 cm^{-1} and 1050 cm^{-1} for C–O–C and Ar–O–R stretching, respectively (Fig. 5). Compared to P200 and C200, P400 and C400 contained more ketones and ethers, which were exhausted after UV irradiation. At same

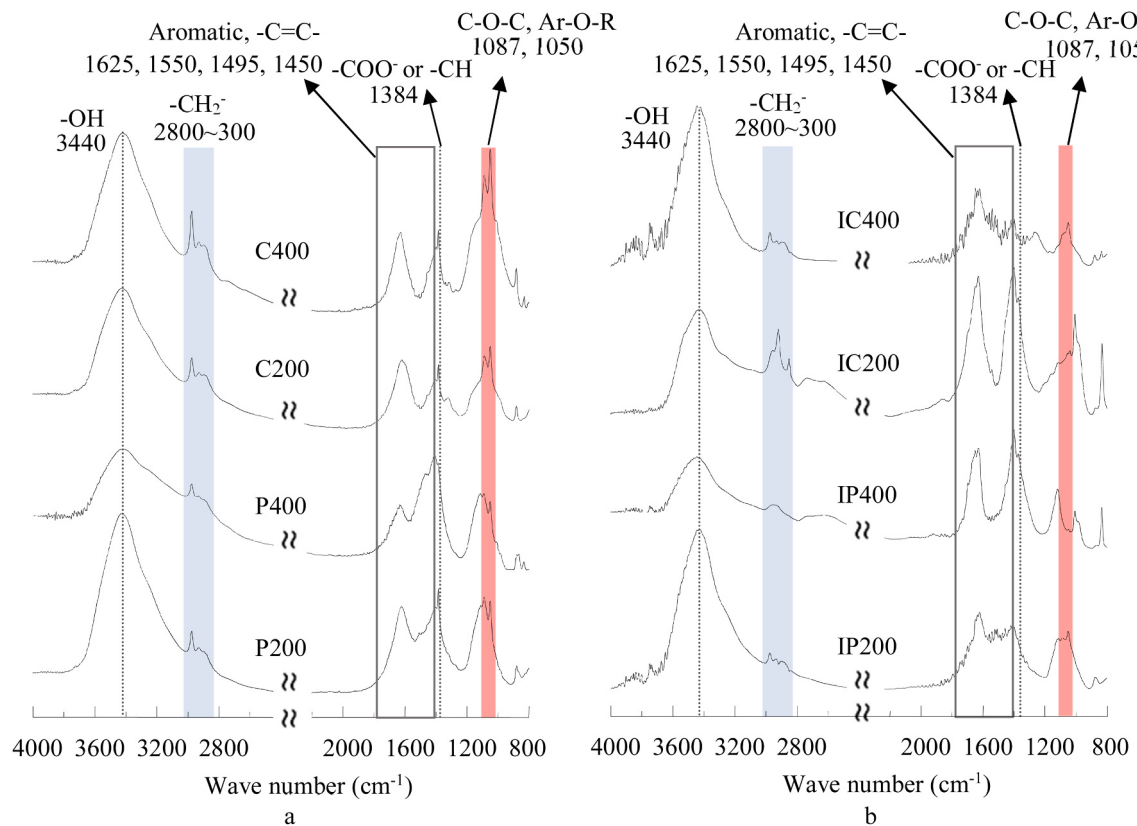


Fig. 5. FTIR spectra of DBC samples before (a) and after (b) 20 h UV light irradiation at 365 nm. IP and IC represent DBCs from peanut shell biochars and from corn straw biochars after a 20 h UV irradiation, respectively.

Table 2
The absorbance of XTT-formazan with model chemicals at 470 nm.

Model chemical	XTT-formazan absorbance	Background absorbance	Absorbance difference
ethylene glycol	0.1682	0.0006	0.1676
dimethyl ether			
ethyl formate	0.2186	0.0027	0.2159
phenyl acetate	0.2355	0.0024	0.2331
glycerol	0.2503	0.0528	0.1975
L-(–)-glyceraldehyde	0.5148	0.0375	0.4773
D-(–)-fructose	0.0657	0.0204	0.0453
propionic acid	0.0021	0.0048	-0.0027
benzoic acid	0.0021	0.0033	-0.0012
diphenyl ether	0.0114	0.0108	0.0006
hydroquinone	1.2372	0.0597	1.1775
1,4-benzoquinone	1.8531	0.1944	1.6587
control	0.0023	0	0.0023

pyrolysis temperature, peanut shell biochars DBCs contained more aliphatic carbonyls, while more ether groups were contained in corn straw biochars DBCs. P400 contained a large number of ketones (14.93 %) than other DBCs, and C400 had more ethers and peroxides. Therefore, ketones and ethers might be the contributing structures to the significant \bullet OH generation from P400 and C400, respectively. The \bullet OH generation from P400 and C400 depended on different pathways.

The aromatic structures under UV can absorb photons and transition to excited state. On one hand, the consumption of aromatic groups within DBCs was evidenced both 1 H NMR spectra (Fig. S3–S6, Table 1) and fluorescence EEM (Fig. 2, Table S3). In addition to the obvious decreasing of fluorescence intensity for DBCs (Fig. 2, Table S3), the olefins/alkyne hydrogen (0.23–5.75 %) and aromatic hydrogen (1.09–48.28 %) of DBCs were non-detectable after UV irradiation (Table 1). On the other hand, according to the reduction of FFA, 1,4-

benzoquinone, hydroquinone, and L- (–)-glyceraldehyde produced 1 O₂ (FFA degradation efficiency > 98 %, Fig. 4b, Table S5). The common structure of these three model chemicals is unsaturated bonds, indicating that unsaturated structures may contribute to 1 O₂ generation. However, it was noticed that not all unsaturated structures could contribute to 1 O₂ generation. That was indicated by the stable concentration of FFA in the presence of diphenyl ether, ethyl formate, phenyl acetate, D- (–)-fructose, propionic acid, and benzoic acid. Thus, it was proposed that aromatic groups within DBC contributed to 1 O₂ generation, while the generation of 1 O₂ was not completely dominated by unsaturated structures.

Generally, phenols could act on electron donor in chemical redox reaction, and thus were deemed the main organic groups in DOM to form O₂[•] by transfer electron to ground state oxygen (3 O₂) [28, 29]. However, the kinetic limitation of spin state of 3 O₂ was ignored in this explanation. The outer electrons of 3 O₂ are specially unpaired with parallel spins in its normal triplet state [30], the direct reaction between 3 O₂ and polyphenols is forbidden by quantum rules [31]. The O₂[•] generation by direct electron transfer between phenolic groups and oxygen may depend on the existence of 1 O₂ in reaction systems, since 1 O₂ is in a quantum state where all electrons are spin paired [31] (Fig. S2). Particularly, 3 O₂ can accept electrons from free radicals [30, 31], which could explain the significant production of O₂[•] by 1,4-benzoquinone (Fig. 4d, Table 2). Excited-state quinone structures could undergo H-atom abstraction reaction to form semiquinone radical [32, 33], and then transfer electron to 3 O₂. Nevertheless, the little phenolic and quinonoid groups within DBCs (Fig. 5, Table 1) were hardly to explain the significant generation of O₂[•] from DBCs, especially in C400 and P400 (Fig. 1a).

It is interesting to notice that corresponding to the abundant OFGs within C400/P400, the formation of O₂[•] was observed in various OFGs model chemical (Figs. 4c, 4d, Table 2), indicating the contribution of

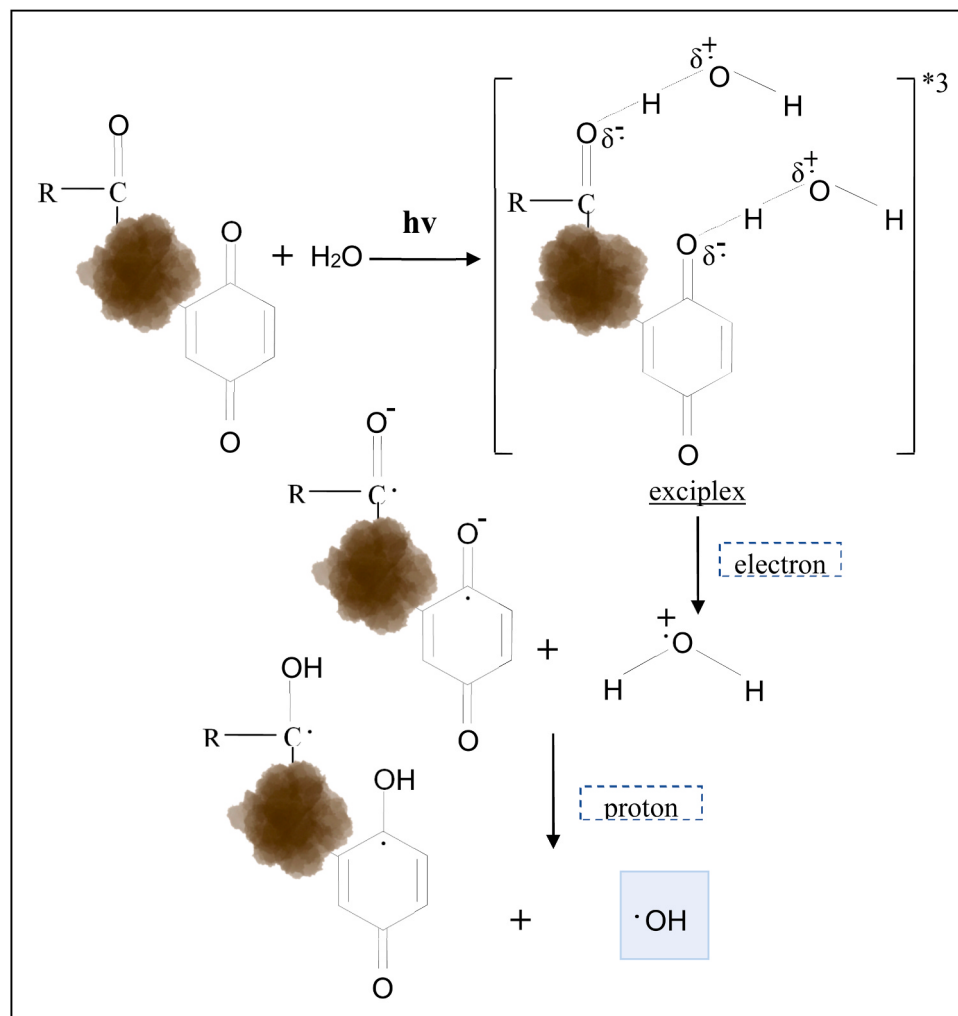


Fig. 6. Mechanisms and processes of •OH production by excited-state carbonyl groups within DBCs.

OFGs to O_2^- generation. Although aliphatic carbonyls, ethers, alcohols, and esters generally do not act on electron donor role in photochemical reactions, these structures also produced O_2^- (Fig. 4d and Table 2). We speculated that the generation of O_2^- from these OFGs might involve a non-electron transfer process.

3.3. Generation mechanism of ROS from DBCs

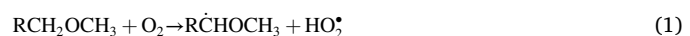
3.3.1. Generation of •OH from carbonyls

The generation of •OH from aliphatic carbonyl groups also involved the cleavage of H_2O like quinones. It was reported that $\text{C}=\text{O}$ groups could promote the oxidation reaction of water, which involved a cleavage of the $\text{O}-\text{H}$ bond [34]. Carbonyls were characterized by $n-\pi^*$ triplet states [33], excited-state carbonyls as an electron-withdrawing group could abstract a H-atom from a water molecule to produce a •OH radical [32,33]. The reaction mechanisms included the form of hydrogen-bonded exciplex [35,36], electron transfer, and ultrafast triplet proton transfer through bound solvent water molecules to excited-state carbonyl oxygen [35,37]. The hydrogen bond between the tautomer and bound water induced H-OH bond cleavage by lowering the activation energy needed for bond dissociation, and the cleavage consequently resulted in •OH generation [37] (Fig. 6).

3.3.2. Ethers generated •OH through the photolysis of H_2O_2

Studies have proposed that the direct photolysis of H_2O_2 contribute to •OH production by DOM in natural waters [38,39]. At present it is

unknown whether the direct contributing structure to the produce H_2O_2 exists. According to both ^1H NMR quantification (Table 1) and FTIR spectra (Fig. 5), the photosensitiveness and consumption of ether groups within DBCs was evidenced. The signals of ethers within DBCs, such as C-O-C and Ar-O-R stretching at 1087 cm^{-1} and 1050 cm^{-1} in FTIR spectra were disappeared after UV irradiation. Meanwhile, the generation of •OH by aliphatic ethers (modeled as ethylene glycol dimethyl ether) was observed. Known photo-excited aliphatic ethers were very reactive and easily to be oxidized to form organic peroxides, and further reacted with water molecule to produce •OH and H_2O_2 (Fig. 7). Thus, it was reasonable that the aliphatic ethers within DBC could produce •OH through the photolysis of H_2O_2 . The generation mechanisms of H_2O_2 were formulated by the photochemical reactions of ethylene glycol dimethyl ether with O_2 , and H_2O (reactions 1–7), and then described in Text S1. Differing from the pathway of •OH generation through H_2O cleavage, which was induced by excited-state carbonyl groups, the photolysis of H_2O_2 depended on the presence of O_2 in reaction systems. Thus, the •OH production by DBCs under UV irradiation in anaerobic condition was further quantified to describe the contribution of O_2 reduction to •OH generation (Fig. 8, Table S6). Compared to the •OH production as indicated by the reduction *p*CBA under aerobic condition, the contribution of O_2 reduction to •OH generation from DBCs was calculated as in the range of 4.03–20.2 %.



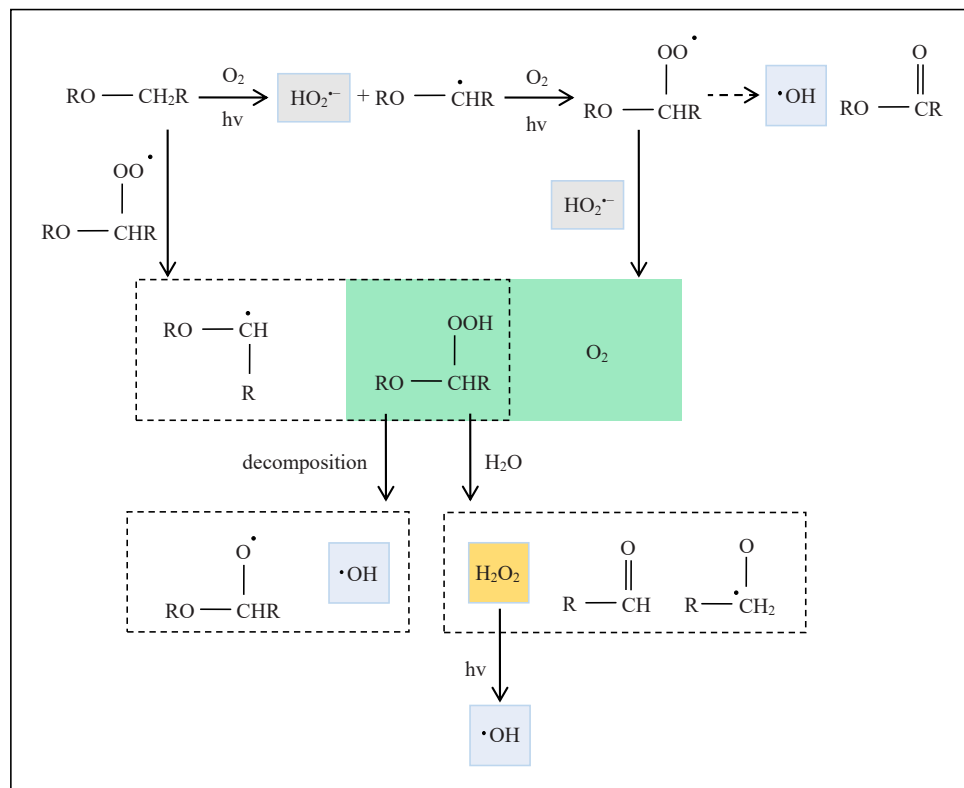


Fig. 7. The potential mechanisms and pathways of $\bullet\text{OH}$ generation by aliphatic ethers within DBCs.

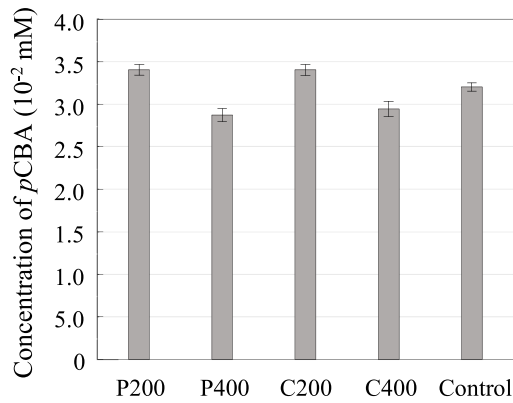
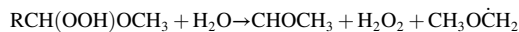
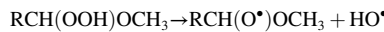
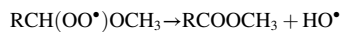
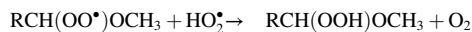
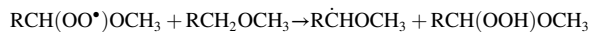
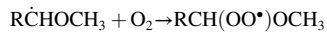


Fig. 8. The production of $\bullet\text{OH}$ from four DBCs under UV irradiation in anaerobic condition as indicated by the reduction $p\text{CBA}$.



3.3.3. Unsaturated structures contributed to $^1\text{O}_2$ generation

The generation of $^1\text{O}_2$ from model chemicals indicated that the unsaturated structures could absorb photons and form triplet excited state DOM ($^3\text{DOM}^*$) through $n\rightarrow\pi^*$ or $\pi\rightarrow\pi^*$ transition. Through intersystem-

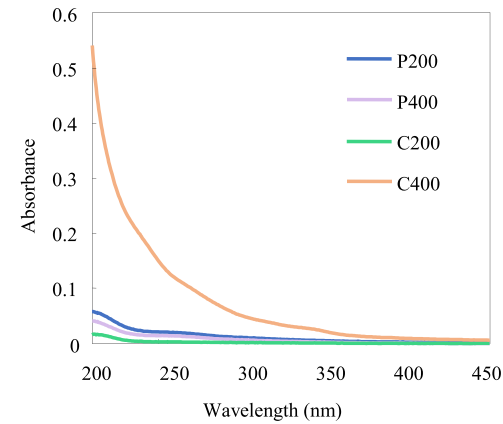


Fig. 9. The UV spectra of 25 mg C/L DBCs.

crossing of $\text{S}\rightarrow\text{T}_\pi, \pi$ transitions or efficient $\text{S}_1\rightarrow\text{T}_1$ intersystem crossing [40,41], the unsaturated structures in triplet excited state could transfer energy to ground state oxygen ($^3\text{O}_2$) to form $^1\text{O}_2$ [42,43].

However, the higher unsaturation (Table 1) and UV adsorption of P200 (Fig. 9, Table S7) did not significantly stimulate the generation of $^1\text{O}_2$ (Fig. 1), suggesting that the degree of unsaturation was essential, but no determination to $^1\text{O}_2$ generation. The transition of electron on the unsaturated bonds might also be dominated by molecular configuration and substituent groups [44,45].

In addition, the production of $^1\text{O}_2$ by DOM positively correlated to the value of $E_2:E_3$ [46,47], which was also observed in this study. C400/P400 with the higher values of $E_2:E_3$ (Table S7), generated more $^1\text{O}_2$ than C200/P200. A higher ratio of $E_2:E_3$ indicates a higher aromaticity [48–52] and lower molecular weight [48,53]. On the one hand, the electrons on unsaturated bonds were through $n\rightarrow\pi^*$ or $\pi\rightarrow\pi^*$ transitioned to the excited state. On the other hand, the smaller sized

excited-state components had faster diffusion so that easier to be quenched by $^3\text{O}_2$ during energy transfer process. Therefore, the two 400 °C DBCs could strongly stimulate $^1\text{O}_2$ generation. It was proposed that the production of $^1\text{O}_2$ is synchronously determined by both the unsaturation of DBC and the energy transfer efficiency between unsaturated groups and $^3\text{O}_2$ molecule.

3.3.4. Formation of O_2^\bullet by non-electron transfer process

It has been proved that ether radical and hydroperoxyl radical (HO_2^\bullet) can be formed in the photooxygenation of aliphatic ethers (reaction 1). As the predecessor of O_2^\bullet , HO_2^\bullet can contribute to the generation of O_2^\bullet through its dissociation ($\text{pK}_a=4.8$) [54,55]. Moreover, the excited state aliphatic carbonyls can undergo the H-atom abstraction reaction [32,33] or the Norrish type I reaction [56] to form alcohol radicals (Text S2), which could participate O_2^\bullet generation by forming HO_2^\bullet [57,58]. The alcohol groups within DBC can also be oxidized by the existing $\bullet\text{OH}$ in reaction system to form alcohol radicals, and then react with O_2 to produce HO_2^\bullet [57–59] (Text S3, reaction 9, 10). In addition, the hydrolysis of esters to form alcohol and phenol is a common pathway for its transformation in aquatic environments [60,61]. Hydrolysis to produce alcohols and phenolic groups may be the participation of esters in O_2^\bullet generation. Therefore, it was reasonable that OFGs, including aliphatic carbonyls, ethers, alcohols, and esters within DBC, could generate O_2^\bullet through the dissociation of HO_2^\bullet . The OFGs within DBC could produce O_2^\bullet by a non-electron transfer process.

4. Conclusion

This study quantified the generation of $\bullet\text{OH}$, O_2^\bullet , and $^1\text{O}_2$ from DBCs under UV irradiation. We analyzed the alterations of chemical structures in DBCs, applied various model chemicals to identify the structures responsible for ROS generation. Results revealed the vital role of OFGs within DBC in the generation of $\bullet\text{OH}$, O_2^\bullet , and $^1\text{O}_2$. A novel non-electron transfer process to generate O_2^\bullet by OFGs within DBC through the dissociation of HO_2^\bullet was proposed. The generation of $^1\text{O}_2$ depended on the aromatic structures within DBC, while simultaneously dominated by molecular configuration, substituent and weight of aromatic groups. Ethers within DBC were identified as the structural source for $\bullet\text{OH}$ generation by H_2O_2 dependent pathway. Moreover, we demonstrated the nonnegligible $\bullet\text{OH}$ generation from aliphatic carbonyls of DBC, the excited-state carbonyl structures could abstract H proton and result in homolytic cleavage of H_2O . Carbonyl structures substantially stimulated the generation of $\bullet\text{OH}$, O_2^\bullet , and $^1\text{O}_2$. Compared to quinonoid groups, the abundant carbonyls within DBC could be the main structures contributing to ROS generation. The stimulation of aliphatic carbonyls within DBC to the generation of ROS deserved more attention. This line of study is essential to establish a general relationship between DBC properties and ROS generation. The new insights revealed in this study may also provide new angles for interpreting the geochemical cycles of DBC and the transformation of contaminants in aquatic environment.

CRediT authorship contribution statement

Lin Wang: Writing – review & editing, Writing – original draft, Project administration, Investigation, Funding acquisition, Conceptualization. **Hao Jiang:** Investigation, Data curation. **Jun Zhang:** Resources, Data curation. **Xinhua He:** Writing – review & editing. **Fangfang Li:** Writing – review & editing, Resources, Funding acquisition. **Jing Feng:** Supervision, Resources. **Bo Pan:** Funding acquisition, Conceptualization.

Declaration of Competing Interest

The authors declare that they have no known competing financial interests or personal relationships that could have appeared to influence the work reported in this paper.

Data availability

Data will be made available on request.

Acknowledgments

This research was supported by the National Natural Scientific Foundation of China (41807382, 41907300 and 42130711), Chinese Post-doctoral Science Foundation (2018M643536), and Yunnan Major Scientific and Technological Projects (202202AG050019).

Appendix A. Supporting information

Supplementary data associated with this article can be found in the online version at doi:10.1016/j.apcatb.2024.123921.

References

- [1] Goldberg, E.D. Black carbon in the environment: properties and distribution. United States: N. P., 1985. Web. <https://www.osti.gov/biblio/5473086>.
- [2] V. Ramanathan, G. Carmichael, Global and regional climate changes due to black carbon, *Nat. Geosci.* 1 (2008) 221–227.
- [3] H. Fu, H. Liu, J. Mao, W. Chu, Q. Li, P.J. Alvarez, X. Qu, D. Zhu, Photochemistry of dissolved black carbon released from biochar: reactive oxygen species generation and phototransformation, *Environ. Sci. Technol.* 50 (2016) 1218–1226.
- [4] C. Chu, R.A. Lundein, C.K. Remucal, M. Sander, K. McNeill, Enhanced indirect photochemical transformation of histidine and histamine through association with chromophoric dissolved organic matter, *Environ. Sci. Technol.* 49 (2015) 5511–5519.
- [5] X. Zhang, J. Li, M.C. Yao, W.Y. Fan, C.W. Yang, L. Yuan, G.P. Sheng, Unrecognized contributions of dissolved organic matter inducing photodamages to the decay of extracellular DNA in waters, *Environ. Sci. Technol.* 54 (2020) 1614–1622.
- [6] K.M. Mostofa, H. Sakugawa, Spatial and temporal variations and factors controlling the concentrations of hydrogen peroxide and organic peroxides in rivers, *Environ. Chem.* 6 (2009) 524–534.
- [7] C. Chang, H. Yang, W. Mu, Y. Cai, L. Wang, L. Yang, H. Qin, In situ fabrication of bismuth oxyiodide ($\text{Bi}_2\text{O}_9\text{I}_3/\text{Bi}_5\text{O}_7\text{I}$) n-n heterojunction for enhanced degradation of triclosan (TCS) under simulated solar light irradiation, *Appl. Catal. B* 254 (2019) 647–658.
- [8] K. Serelis, N. Mantzos, D. Meintani, I. Konstantinou, The effect of biochar, hydrochar particles and dissolved organic matter on the photodegradation of metribuzin herbicide in aquatic media, *J. Environ. Chem. Eng.* 9 (2021) 105027.
- [9] L. Li, X. Wang, H. Fu, X. Qu, J. Chen, S. Tao, D. Zhu, Dissolved black carbon facilitates photoreduction of $\text{Hg}(\text{II})$ to $\text{Hg}(\text{0})$ and reduces mercury uptake by lettuce (*Lactuca sativa L.*), *Environ. Sci. Technol.* 54 (2020) 11137–11145.
- [10] S. Yang, X. Ge, Y. Li, H. Ding, Y. Li, C. Wang, A. Lu, Light-induced coupling process of Fe redox cycling and natural dissolved organic matters oxidative decomposition at goethite surface: Key role of reactive oxidative species, *Chem. Geol.* 603 (2022) 120928.
- [11] E. Cabisco Català, J. Tamarit Sumalla, J. Ros, Salvador, Oxidative stress in bacteria and protein damage by reactive oxygen species, *Int. Microbiol.* 3 (2000) 3–8.
- [12] J. Gehring, B. Treppka, N. Klinkenberg, H. Bronner, D. Schleheck, S. Polarz, Sunlight-triggered nanoparticle synergy: teamwork of reactive oxygen species and nitric oxide released from mesoporous organosilica with advanced antibacterial activity, *J. Am. Chem. Soc.* 138 (2016) 3076–3084.
- [13] M. Aeschbacher, M. Sander, R.P. Schwarzenbach, Novel electrochemical approach to assess the redox properties of humic substances, *Environ. Sci. Technol.* 44 (2010) 87–93.
- [14] N. Ratasuk, M.A. Nanny, Characterization and quantification of reversible redox sites in humic substances, *Environ. Sci. Technol.* 41 (2007) 7844–7850.
- [15] L. Sun, J. Qian, N.V. Blough, K. Mopper, Insights into the photoproduction sites of hydroxyl radicals by dissolved organic matter in natural waters, *Environ. Sci. Technol. Lett.* 2 (2015) 352–356.
- [16] Y. Li, J. Niu, E. Shang, J.C. Crittenden, Synergistic photogeneration of reactive oxygen species by dissolved organic matter and C_60 in aqueous phase, *Environ. Sci. Technol.* 49 (2015) 965–973.
- [17] Y. Pi, J. Schumacher, M. Jekel, The use of para-chlorobenzoic acid (pCBA) as an ozone/hydroxyl radical probe compound, *Ozone: Sci. Eng.* 27 (2005) 431–436.
- [18] G. Bartosz, Use of spectroscopic probes for detection of reactive oxygen species, *Clin. Chim. Acta* 368 (2006) 53–76.
- [19] J. Lee, J.D. Fortner, J.B. Hughes, J.H. Kim, Photochemical production of reactive oxygen species by C_60 in the aqueous phase during UV irradiation, *Environ. Sci. Technol.* 41 (2007) 2529–2535.
- [20] Y. Zhang, R. Del Vecchio, N.V. Blough, Investigating the mechanism of hydrogen peroxide photoproduction by humic substances, *Environ. Sci. Technol.* 46 (2012) 11836–11843.
- [21] Y. Zhang, Q. Xie, Z. Xia, G. Gui, F. Deng, Fulvic Acid Reduced GO and Phthalocyanine nanorods as reaction platform for simultaneous determination of catechol, hydroquinone, phenol and p-nitrophenol, *J. Electrochem. Soc.* 166 (2019) B1293.

[22] H. Li, Y. Li, C. Li, Characterization of humic acids and fulvic acids derived from sewage sludge, *Asian J. Chem.* 25 (2013).

[23] S.E. Page, W.A. Arnold, K. McNeill, Assessing the contribution of free hydroxyl radical in organic matter-sensitized photohydroxylation reactions, *Environ. Sci. Technol.* 45 (2011) 2818–2825.

[24] S. Canonica, U. Jans, K. Stemmler, J. Hoigne, Transformation kinetics of phenols in water: photosensitization by dissolved natural organic material and aromatic ketones, *Environ. Sci. Technol.* 29 (1995) 1822–1831.

[25] K.A. Thorn, D.W. Folan, P. MacCarthy, Characterization of the International Humic Substances Society standard and reference fulvic and humic acids by solution state carbon-13 (^{13}C) and hydrogen-1 (^1H) nuclear magnetic resonance spectrometry, *Water Res. Investig. Rep.* 89 (1989) 1–93.

[26] N. Fuloria, S. Fuloria, Structural elucidation of small organic molecules by 1D, 2D and multi-dimensional-solution NMR spectroscopy, *Anal. Bioanal. Tech.* 11 (2013) 1–8.

[27] A. Piccolo, P. Conte, E. Trivellone, B. Van Lagen, P. Buurman, Reduced heterogeneity of a lignite humic acid by preparative HPSEC following interaction with an organic acid. Characterization of size-separates by Pyr-GC-MS and ^1H NMR spectroscopy, *Environ. Sci. Technol.* 36 (2002) 76–84.

[28] D. Zhang, S. Yan, W. Song, Photochemically induced formation of reactive oxygen species (ROS) from effluent organic matter, *Environ. Sci. Technol.* 48 (2014) 12645–12653.

[29] Y. Zhang, N.V. Blough, Photoproduction of one-electron reducing intermediates by chromophoric dissolved organic matter (CDOM): relation to O_2 and H_2O_2 photoproduction and CDOM photooxidation, *Environ. Sci. Technol.* 50 (2016) 11008–11015.

[30] C. John Danilewicz, Role of tartaric and malic acids in wine oxidation, *J. Agric. Food Chem.* 62 (2014) 5149–5155.

[31] A.L. Waterhouse, V.F. Laurie, Oxidation of wine phenolics: a critical evaluation and hypotheses, *Am. J. Enol. Vitic.* 57 (2006) 306–313.

[32] S. Beck, L. Brus, Photooxidation of water by p-benzoquinone, *J. Am. Chem. Soc.* 104 (1982) 1103–1104.

[33] A. Pochon, P.P. Vaughan, D. Gan, P. Vath, N.V. Blough, D.E. Falvey, Photochemical oxidation of water by 2-methyl-1, 4-benzoquinone: evidence against the formation of free hydroxyl radical, *J. Phys. Chem. A* 106 (2002) 2889–2894.

[34] Y. Lin, K.-H. Wu, Q. Lu, Q. Gu, L. Zhang, B. Zhang, D. Su, M. Plodinec, R. Schlogl, S. Heumann, Electrocatalytic water oxidation at quinone-on-carbon: a model system study, *J. Am. Chem. Soc.* 140 (2018) 14717–14724.

[35] A.M. Ribeiro, A.R. Bertotti, J.C. Netto-Ferreira, Phenolic hydrogen abstraction by the triplet excited state of thiocromanone: a laser flash photolysis study, *J. Braz. Chem. Soc.* 21 (2010) 1071–1076.

[36] J. Zhao, H. Yao, J. Liu, M.R. Hoffmann, New excited-state proton transfer mechanisms for 1, 8-dihydroxydibenzo [a, h] phenazine, *J. Phys. Chem. A* 119 (2015) 681–688.

[37] L. Sun, Study of photochemical formation of hydroxyl radical in natural waters, (2015). Doctor of Philosophy (PhD), Dissertation, Chemistry & Biochemistry, Old Dominion University, DOI: 10.25777/6jqz-e603.

[38] G. McKay, F.L. Rosario-Ortiz, Temperature dependence of the photochemical formation of hydroxyl radical from dissolved organic matter, *Environ. Sci. Technol.* 49 (2015) 4147–4154.

[39] K.M. Mostafa, H. Sakugawa, Spatial and temporal variation of hydrogen peroxide in stream and river waters: Effect of photo-bio-physio-chemical processes of aquatic matters, *Geochim. Cosmochim. Acta* 67 (2003) A309.

[40] D.R. Kearns, W.A. Case, Investigation of singlet→ triplet transitions by the phosphorescence excitation method. III. Aromatic ketones and aldehydes, *J. Am. Chem. Soc.* 88 (1966) 5087–5097.

[41] T. Itoh, H. Baba, T. Takemura, Phosphorescence Emissions and nonradiative properties of vapors of aromatic carbonyl compounds at low pressure, *Bull. Chem. Soc. Jpn.* 51 (1978) 2841–2846.

[42] S.B. Partanen, P.R. Erickson, D.E. Latch, K.J. Moor, K. McNeill, Dissolved organic matter singlet oxygen quantum yields: evaluation using time-resolved singlet oxygen phosphorescence, *Environ. Sci. Technol.* 54 (2020) 3316–3324.

[43] A. Fede, A.M. Grannas, Photochemical production of singlet oxygen from dissolved organic matter in ice, *Environ. Sci. Technol.* 49 (2015) 12808–12815.

[44] C.A. Parker, Photoluminescence of Solutions: with applications to photochemistry and analytical chemistry, *J. Chem. Educ.* 46 (1969) 111.

[45] S.G. Schulman, *Fluorescence and Phosphorescence Spectroscopy: Physicochemical Principles and Practice*, Elsevier, 2017.

[46] R.M. Dalrymple, A.K. Carfagno, C.M. Sharpless, Correlations between dissolved organic matter optical properties and quantum yields of singlet oxygen and hydrogen peroxide, *Environ. Sci. Technol.* 44 (2010) 5824–5829.

[47] S. Mostafa, F.L. Rosario-Ortiz, Singlet oxygen formation from wastewater organic matter, *Environ. Sci. Technol.* 47 (2013) 8179–8186.

[48] J. Peuravuori, K. Pihlaja, Molecular size distribution and spectroscopic properties of aquatic humic substances, *Anal. Chim. Acta* 337 (1997) 133–149.

[49] J.K. Edzwald, W.C. Becker, K.L. Wattier, Surrogate parameters for monitoring organic matter and THM precursors, *J. -Am. Water Works Assoc.* 77 (1985) 122–132.

[50] Y.P. Chin, G.R. Aiken, K.M. Daniels, Binding of pyrene to aquatic and commercial humic substances: the role of molecular weight and aromaticity, *Environ. Sci. Technol.* 31 (1997) 1630–1635.

[51] S.J. Traina, J. Novak, N.E. Smeek, An ultraviolet absorbance method of estimating the percent aromatic carbon content of humic acids, *J. Environ. Qual.* 19 (1990) 151–153.

[52] J. Novak, G. Mills, P. Bertsch, Estimating the percent aromatic carbon in soil and aquatic humic substances using ultraviolet absorbance spectrometry, *J. Environ. Qual.* 21 (1992) 144–147.

[53] H. De Haan, T. De Boer, Applicability of light absorbance and fluorescence as measures of concentration and molecular size of dissolved organic carbon in humic Lake Tjeukemeer, *Water Res.* 21 (1987) 731–734.

[54] B.H. Bielski, D.E. Cabelli, R.L. Arudi, A.B. Ross, Reactivity of HO_2/O_2 radicals in aqueous solution, *J. Phys. Chem. Ref. data* 14 (1985) 1041–1100.

[55] A.L. Rose, T.D. Waite, Reduction of organically complexed ferric iron by superoxide in a simulated natural water, *Environ. Sci. Technol.* 39 (2005) 2645–2650.

[56] N.J. Turro, V. Ramamurthy, J.C. Scaiano, *Modern molecular photochemistry of organic molecules*, Viva Books University Science Books, Sausalito, 2017.

[57] B. Grote, Application of advanced oxidation processes (AOP) in water treatment, 37th Annual old Water Industry Operations Workshop Parklands, Gold. Coast (2012) 17–23.

[58] C. Zhu, F. Zhu, D.D. Dionysiou, D. Zhou, G. Fang, J. Gao, Contribution of alcohol radicals to contaminant degradation in quenching studies of persulfate activation process, *Water Res.* 139 (2018) 66–73.

[59] E. Popov, M. Mametkuliyev, D. Santoro, L. Liberti, J. Eloranta, Kinetics of UV– H_2O_2 advanced oxidation in the presence of alcohols: the role of carbon centered radicals, *Environ. Sci. Technol.* 44 (2010) 7827–7832.

[60] Y. Pan, D.C. Tsang, Y. Wang, Y. Li, X. Yang, The photodegradation of polybrominated diphenyl ethers (PBDEs) in various environmental matrices: kinetics and mechanisms, *Chem. Eng. J.* 297 (2016) 74–96.

[61] S. Rayne, P. Wan, M. Ikonomou, Photochemistry of a major commercial polybrominated diphenyl ether flame retardant congener: 2, 2, 4, 4', 5, 5'-hexabromodiphenyl ether (BDE153), *Environ. Int.* 32 (2006) 575–585.